Controlling on-surface polymerization by hierarchical and substrate-directed growth

L. Lafferentz[1,3], V. Eberhardt[2], C. Dri[3], C. Africh[3],

G. Comelli[3,4], F. Esch[3§], S. Hecht[2*], and L. Grill[1*]

[1] *Department of Physical Chemistry, Fritz-Haber-Institute of the Max-Planck-Society, 14195 Berlin, Germany*

[2] *Department of Chemistry, Humboldt-Universität zu Berlin, 12489 Berlin, Germany*

[3] *IOM-CNR Laboratorio TASC, Area Science Park, 34149 Basovizza-Trieste, Italy*

[4] *Physics Department and CENMAT, University of Trieste, 34127 Trieste, Italy*

[§] *present address: Chemistry Department, Technische Universität München, 85748 Garching, Germany*

**) Corresponding authors: sh@chemie.hu-berlin.de and lgr@fhi-berlin.mpg.de*

Contents

Synthesis

General Methods. Chemicals were purchased from Acros and were used as received. Column chromatography was carried out with silica gel 60 A (40-63 μm, 230-400 mesh) by Merck. The porphyrin filtrations were done with aluminium oxide (50-200 μm, Acros). The ^{1}H-NMR experiments were recorded in the reported solvents with a Bruker DPX 300 spectrometer at room temperature with the residual protonated solvent signal as internal standard, i.e. $\delta(CH_2Cl_2)$ = 5.32 ppm. UPLC-MS measurements were performed on a Waters Aquity with aWaters Photo diode array detector 2996, a Waters ESI-MS Detector LCT Premier XE and an Aquity BEH Phenylcolumn (1.7 μm, 2.0 x 150 mm).

Synthesis

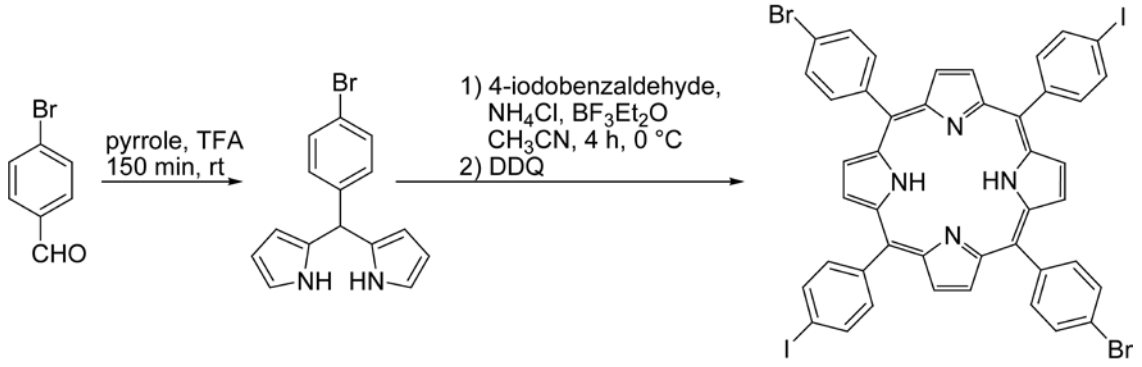

5-(4-Bromophenyl)dipyrromethane was synthesized using a procedure by Lindsey and coworkers [1]. 4-Bromobenzaldehyde (925 mg, 5 mmol) was dissolved in pyrrole (13.9 mL, 200 mmol) in an argon atmosphere and degassed by bubbling argon through the solution for 20 min. Trifluoroacetic acid (0.05 mL, 0.7 mmol) was added and the solution was stirred at room temperature for 150 min. An aqueous NaOH-solution (1 M, 10 mL) and 20 mL of methylene chloride were added. The aqueous layer was extracted once with methylene chloride and the combined organic phases were washed with water and brine twice and dried over $MgSO_4$. After evaporation of excess pyrrole, the remaining black resin was chromatographed (silica gel, methylene chloride/petrolether/triethylamine 66/33/1), yielding 0.65 g of the product as a grey solid (43% yield). **^{1}H-NMR** (CD_2Cl_2, 300 MHz): δ (ppm) = 5.35 (s, 1H, *meso*-C-*H*), 5.77 (m, 2H, Pyr-*H*), 6.04 (dd, 2H, Pyr-*H*), 6.62 (m, 2H, Pyr-*H*), 7.01 (d, J^3 = 8.2 Hz, 2H, Ar-*H*), 7.37 (d, J^3 = 8.4 Hz, 2H, Ar-*H*), 7.94 (br s, 2H, N-*H*). **UPLC-MS** (flow = 0.6 mL/min; grad.:

CH_3OH/H_2O 40/60 with 0.1 vol% formic acid - CH_3OH/H_2O 80/20 with 0.1 vol% formic acid): t_R = 4.48 min, >99 % peak area (λ = 254 nm). **HRMS:** ESI(+): calcd for $C_{15}H_{14}N_2Br$: *m/z* = 301.0340; found: *m/z* = 301.0286. The analytical data were in agreement with the literature [2].

5,15-Bis(4'-bromophenyl)-10,20-bis(4'-iodophenyl)porphyrin (*trans*-Br_2I_2TPP) was prepared adapting a procedure developed by Lindsey et al. [3]. In an argon atmosphere 5-(4-bromophenyl)dipyrromethane (602 mg, 2.00 mmol) was dissolved in 200 mL of acetonitrile and NH_4Cl (1.07 g, 20.0 mmol) was added. The mixture was degassed by bubbling argon through the solution for 15 min and cooled to 0 °C. 4-Iodobenzaldehyde (0.464 g, 2.00 mmol) and $BF_3 \cdot Et_2O$ (0.025 mL, 0.200 mmol) were added and the mixture was stirred at 0 °C for 4 h. Then, 2,3-dichloro-5,6-dicyano-1,4-benzoquinone (910 mg, 4.00 mmol) was added and the reaction was stirred at room temperature for 12 h. Filtration of a solution in methylene chloride through a pad of neutral aluminum oxide gave a purple/black solid material. Column chromatography (silica gel, petrolether/methylene chloride/triethylamine 80/20/1) gave a slightly impure product, which was further purified by another round of column chromatography (silica gel, petrolether/methylene chloride/triethylamine 90/10/1). The product was obtained as a purple solid (13 mg) in 1% yield. **^{1}H-NMR** (CD_2Cl_2, 300 MHz): δ (ppm) = -2.89 (s, 2H, N-*H*), 7.96 (d, ^{3}J(*H*,*H*) = 9 Hz, 4H, Ar-*H*), 7.99 (d, ^{3}J(*H*,*H*) = 9 Hz, 4H, Ar-*H*), 8.13 (d, ^{3}J(*H*,*H*) = 9 Hz, 4H, Ar-*H*), 8.17 (d, ^{3}J(*H*,*H*) = 9 Hz, 4H, Ar-*H*), 8.91 (s, 8H, pyr-*H*). **UPLC-MS** (flow = 0.6 mL/min; CH_3CN/H_2O 90/10 with 0.1 vol% formic acid): t_R = 5.42 min, 95.4 % peak area (λ = 410 nm). **HRMS:** ESI(+): calcd for $C_{44}H_{27}N_4Br_2I_2$: *m/z* = 1022.8692; found: *m/z* = 1022.8723.

Stepwise hierarchical growth in overview images

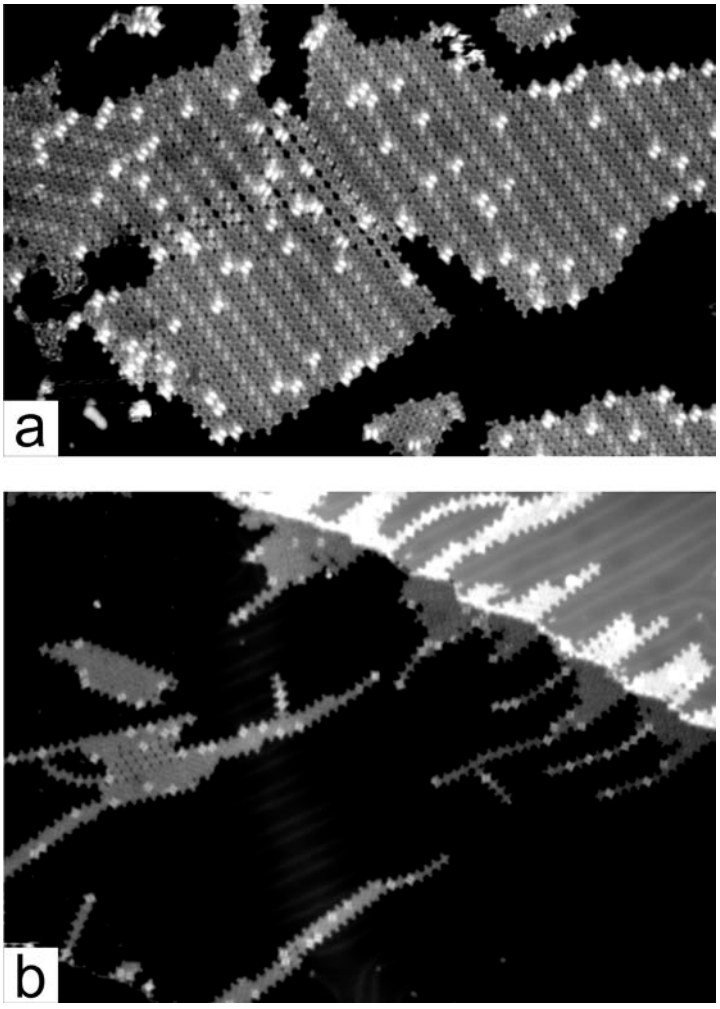

Figure S1: LT-STM images of trans-Br_2I_2TPP molecules on Au(111) taken directly after molecule deposition onto a sample at room temperature (a; 50×80 nm^2) and after heating the sample to 120 °C for 5 minutes (b; 85×120 nm^2). Both images were taken at 1 V bias and 0.1 nA tunneling current.

Figure S1 shows overview STM images of *trans*-Br_2I_2TPP molecules on Au(111) directly after deposition of the molecules onto the sample kept at RT, i.e. without heating of the sample (a), and after the first heating step at 120 °C (b). Overview images of the surface after heating to 250 °C are presented in Fig.S2, comparing the *trans*-Br_2I_2TPP molecules (a) with Br_4TPP (b). The solid arrow in (a) denotes a network area, in which the resolution is reduced by adatoms filling the gaps; the dashed arrow points out two former chains in a curved shape that causes a mismatch

of the building blocks in the vicinity. Non-orthogonal structures, such as triangular and pentagonal defects (marked in (b)), are a result of the flexibility of the precursors (discussed below in the context of regularity). Note that the TPP molecules can appear as dark or bright protrusions in STM images, which we assign to planar and saddle-shaped conformations of the porphyrin core[4].

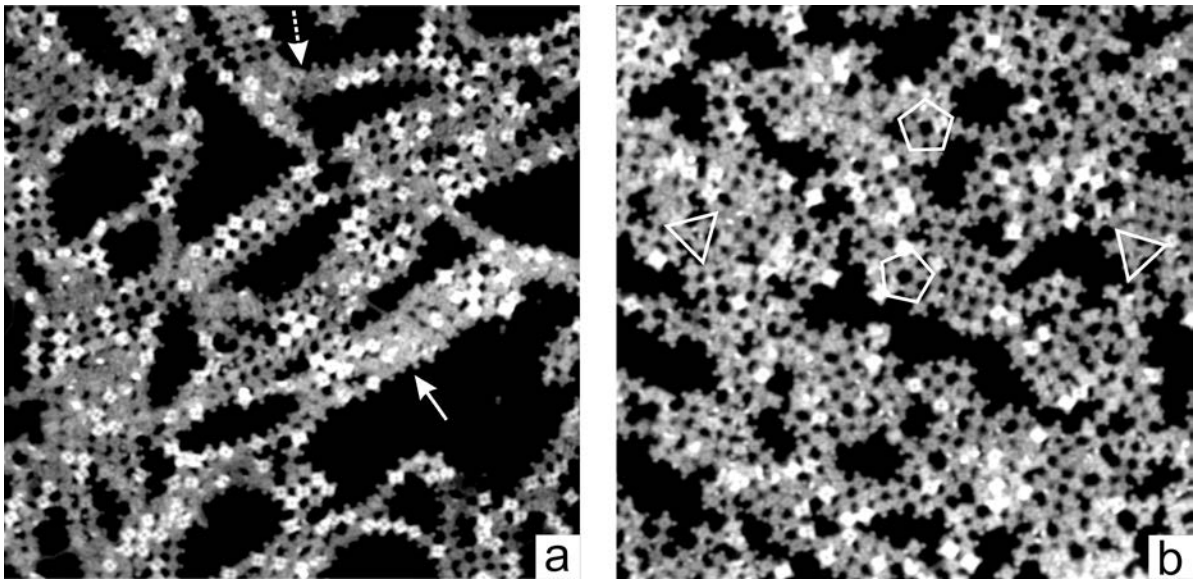

Figure S2: LT-STM images of trans-Br_2I_2TPP (a) and Br_4TPP (b) after heating the Au(111) sample to 250 °C for 5 minutes (parameters for both images: 1 V bias voltage and 0.1 nA tunneling current, size 62.5 × 62.5 nm^2). Superimposed triangles and pentagons in (b) indicate the corresponding defects.

Reaction pathways

The advantage of hierarchical growth by choosing a particular reaction pathway is illustrated schematically in Fig.S3 where the sequential growth of a square-shaped tetramer by first building dimers and subsequently connecting two dimers sideways is marked by red arrows. Although only very few initial bond formation steps are considered, the polymerization process is – due to reduced number of reaction pathways – much more efficient than non-hierarchical polymerization that allows monomer attachment randomly at four sites in all steps (black arrows).

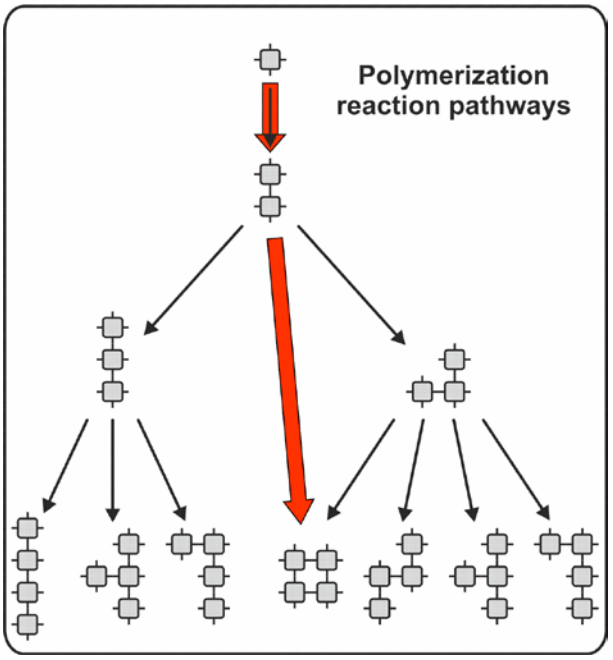

Figure S3: Simplified sketch of the possible reaction pathways during the initial polymerization stages of a molecule with four potential connection sites. Efficient formation of a regular 2D squared arrangement is obtained by choosing a specific reaction pathway (marked by red arrows).

Identification of halogen substituents

To identify the two different halogen substituents on the *trans*-Br_2I_2TPP molecules, we utilized their characteristic apparent heights in STM images. For this, we compared the measured heights to those obtained from similar porphyrin building blocks that were synthesized with only one type of halogen atom. Figure S4 shows the height profiles across single molecules with different substituent arrangements. The two molecules used for comparison (at the center/right of the figure) consist of a porphyrin core with bromophenyl (center) or iodophenyl (right) groups at the *meso* position in a *trans* configuration. However, unlike the *trans*-Br_2I_2TPP molecule, they do not possess halogen substituents in the orthogonal direction, where phenyl (center) and mesityl (right) groups are attached. The good agreement of the height profiles of the bromine atoms with the lower protrusions on the *trans*-Br_2I_2TPP side groups and likewise of the iodine atoms with the higher protrusions allow the identification of the substituents. The brighter protrusions (apparent height of 1.7 ± 0.1 Å) thus represent the iodine substituents, while the bromine legs appear lower (1.3 ± 0.1 Å). On the other hand, a very different appearance without a distinct protrusion is observed for activated legs (i.e. after halogen dissociation)[5].

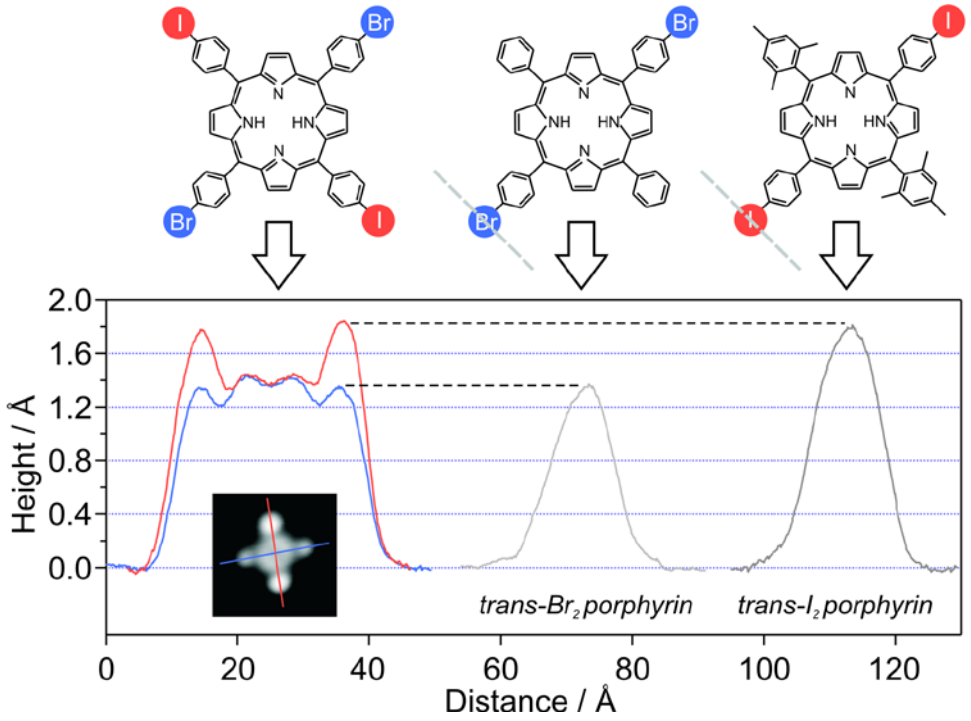

Figure S4: Height profiles and chemical structures of the molecules used for the assignation of the two halogen types to the side groups of trans-Br_2I_2TPP. Left: trans-Br_2I_2TPP, center and right: singly-substituted porphyrin derivatives for comparison. The position of the height profiles over the halogen atoms are indicated by the dashed grey lines.

Fingerprint of the covalent bond

In a previous study we found that the newly formed covalent bond between two porphyrin derivatives causes a characteristic resonance at 3 eV above the Fermi energy[5]. As found by theoretical calculations, this peak stems from the interaction of the π orbitals, which can only be explained by a covalent bond and not by any other type of intermolecular interaction. Thus, it represents a convenient fingerprint for the covalent nature of the formed bonds as it can be probed locally for individual molecules by STM spectroscopy. The same fingerprint is found for interconnected *trans*-Br_2I_2TPP molecules, where it is visualized by bias-dependent imaging (Fig.S5). The similarity with the previously studied Br_nTPP molecules[5] confirms the identical intermolecular bonds in the present case. While connected molecules appear in homogeneous contrast at low bias voltages, bright protrusions become visible at the intermolecular connection if the bias voltage is raised to 3 V (marked by an arrow in Fig.S5b).

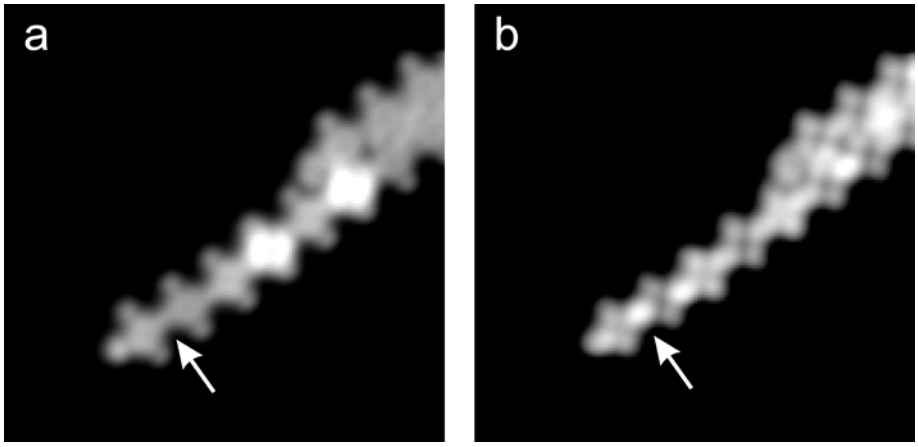

Figure S5: STM images of molecular chains formed by heating the Au(111) sample prepared with trans-Br_2I_2TPP precursors to 120°C for 5 min. (a) and (b) show the same area at a bias voltage of 1 V and 3 V, respectively and a tunneling current of 0.1 nA. Image size 15×15 nm^2. The arrow indicates a bond position that appears as a protrusion in (b).

Enhanced regularity by hierarchical growth

The concept of hierarchical growth allows the formation of more sophisticated structures by selective activation of different dormant reactive sites on molecular building blocks. However, it can also serve to enhance the *regularity* of the produced networks.

In arrays formed from the one-step-connecting Br_4TPP a frequent feature are non-orthogonal links, resulting in triangles or pentagons (see Fig.S2b). They originate from the flexibility and different possible conformations of the precursor molecules and the low barrier of the connection reaction. Thus, if a molecule is already linked to a neighbouring building block and finds another reaction partner (with one of its remaining reactive sites) and does so while thermally bending, then this new bond can deviate from the ideal square geometry. As a consequence, these non-orthogonal structures lead to further mismatch, leaving activated building blocks in the vicinity of the defect without a reaction partner. Thus, the regularity decreases and the network size is lowered. Note that the process produces non-reversible covalent bonds[6] and therefore prohibits the possibility for self-repair.

By following our strategy of hierarchical growth, the network formation is separated into two consecutive steps. In the first step, the dissociation of iodine substituents leads to the formation of linear porphyrin chains with intact bromine-protected groups pointing sideways. In this step,

there is no possibility for defects of the type discussed above. The covalently bound chains favor the agglomeration to islands in which they are arranged in a parallel fashion. The equidistant side groups interlock, resembling gears and therefore minimizing the distance between the polymers. This is the starting point for the second step, the dissociation of the bromine atoms and a connection of the chains to networks. The parallel and one-on-one pre-arrangement of the potentially reactive sites markedly reduces number of the above-mentioned defects.

There is however one caveat: if parallel running chains bend, as they are prone to do when they become longer, then this can again cause mismatch, because in the curved sections the one-on-one matching between convex and concave faces can be hindered. This can then lead to the formation of pentagons as shown in Fig.S6f.

Network size

To understand the influence of sequential activation and substrate-directed diffusion on the quality of the networks, their size is measured for different preparations. This task requires a statistical analysis of the networks, i.e. to count the number of building blocks in each network, and in particular a definition of what is considered a network. Simply counting all connected monomers is not sufficient, because the objective of the *trans*-Br_2I_2TPP molecules is to form *two-dimensional* architectures realizing all possible interconnections, i.e. up to four at each building block. However, the size of a network is generally limited by two types of defects: Missing and incorrectly formed bonds. The former is caused by bonds that are not realised (see Fig.S6b) or missing monomer building blocks (e), whereas the latter originates from the different conformations of the porphyrin monomers (c) and/or bending/mismatch of the net (f). Note that an STM image containing triangular and pentagonal defects, sketched in (c) and (f), respectively, is presented in Fig.S2b.

In this study, we define two counting conditions:

1) *Each molecule in a network must be part of a 2x2 square sub-unit* to be considered. For instance, Fig.S6a shows a case where all connected building blocks are counted. In contrary, only 6 molecules of the network are considered in (e), because (1) is not fulfilled by the two molecules attached at the left.

2) *A molecule is only counted, if all possible bonds to the super-network are realized*. This is why in Fig.S6d two monomers are disqualified.

It is important to note that the determination of network sizes can be complicated by a low resolution of the STM images. Furthermore, networks that leave the boundaries of an image have to be disregarded. Consequently, we considered only such networks for the statistical analysis that are imaged with intact bonds and porphyrin cores at low bias voltage.

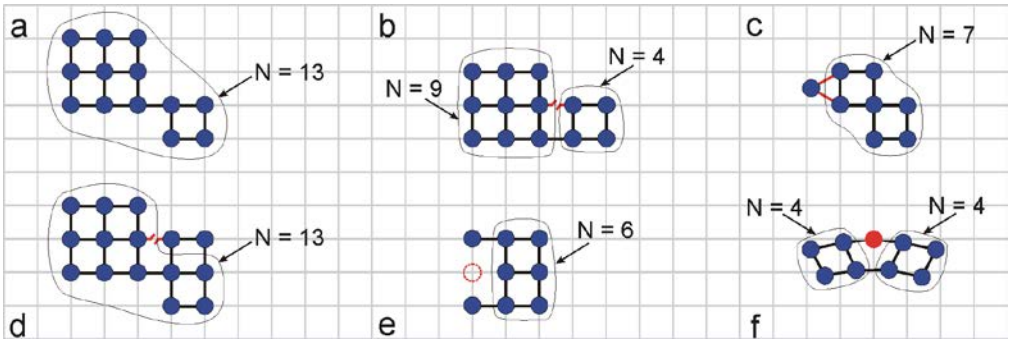

Figure S6: Models of networks formed by trans-Br_2I_2TPP molecules. N indicates the number of monomers counted for a given network (contained by the line). (b-f) exemplify the types of defects that limit a network's size. If there are different possibilities to count, the biggest network is selected, for instance N=13 in (d).

Heterogeneous growth with Br_4TPP and DBTF

The covalent linking of a mixture of *trans*-Br_2I_2TPP and DBTF molecules (Fig.4 in the manuscript) illustrates the strength of the hierarchical growth process as high selectivity is achieved by the stepwise activation of iodine and bromine substituents. The use of Br_4TPP on the other hand, in combination with DBTF molecules, does not allow such a hierarchical process, because only one type of halogen substituent is present, thus covalent linking occurs on all sites under the same conditions. Selectivity in the heterogeneous connection can therefore not be achieved, which becomes clear in Fig.S7. While the covalent linking was successful and networks of mixed composition are obtained, all bonding sites at the TPP building blocks are equivalent for DBTF attachment during the chemical reaction. In particular, DBTF molecules are often found to be connected to the TPP molecules in orthogonal geometries (marked by arrows in Fig.S7). Such configurations are only very rarely found for the case of hierarchical growth (see statistics in Fig.4c of the manuscript).

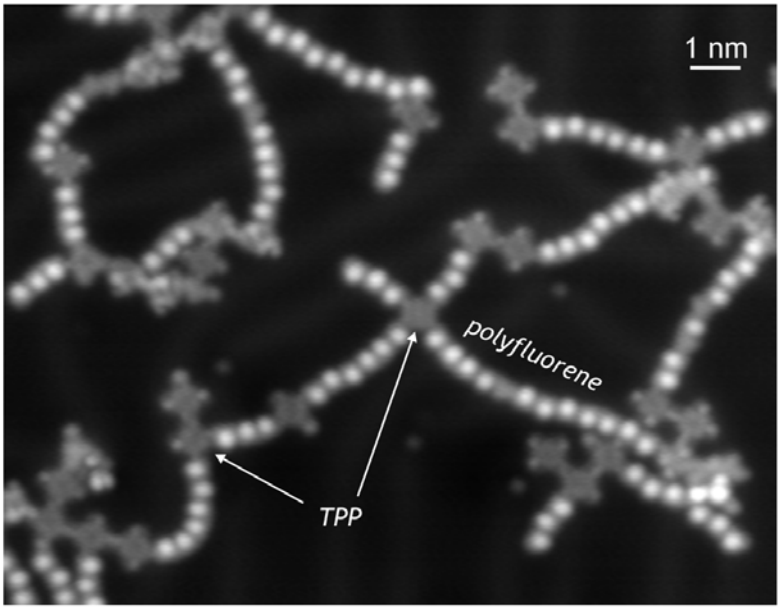

Figure S7: STM image of a covalently bound mixture of Br_4TPP and DBTF molecules on Au(111). After deposition of the two molecular species, the sample was heated at 250°C to induce activation of the Br sites and subsequent polymerization.

Au(100) surface

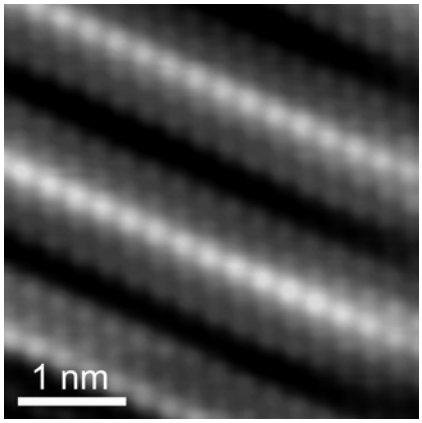

Figure S8: STM image of the Au(100) surface with atomic resolution (bias voltage = 100 mV; I = 40 nA).

The Au(100) surface, after being prepared by conventional sputtering and annealing cycles, exhibits the characteristic corrugated structure as shown in the STM image of Fig.S8. The vertical corrugation of the atoms and the thus created rows at a distance of 14.4 Å can be clearly

seen. This reconstruction, which can in a first approximation be described as a (5×1) structure, is found to exhibit a (5×20) periodicity, in which the topmost layer is close-packed in a quasi-hexagonal superstructure[7,8]. This layer is incommensurate with the square substrate of the second layer underneath. It exhibits a very weak corrugation of only 0.65 Å at maximum[8], which renders it promising as a template surface for the polymerization experiments.

Intramolecular binding angles in networks on Au(100)

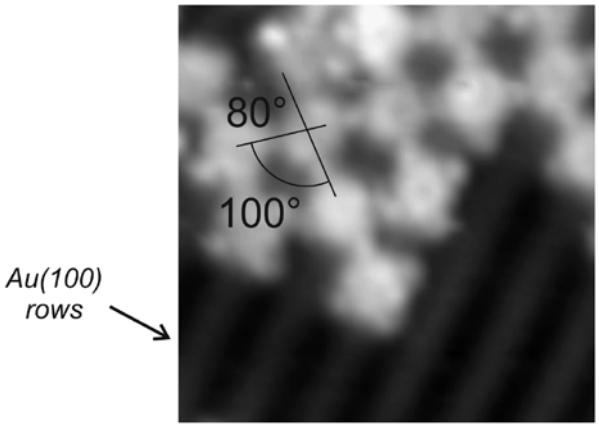

Figure S9: STM image of a small network formed from trans-Br_2I_2TPP on Au(100). The intramolecular binding angle of 100° is indicated (number of counted networks: 50).

The intramolecular binding angle of around 90° is presented in Fig.5. For small structures of a few monomers, this angle is found to be around 101°, due to the dominating molecule-surface interaction. An example is shown in Fig.S9 with a network of only few monomers and an angle of 100°. While we observed 2×2 networks with bond angles of around 100°, slightly larger 3×3 networks are already rectangular and thus are stabilized by the interaction between the molecules. Note that these large angles for small networks always open along the atomic rows of the substrate, while perpendicular to the rows the complementary angles below 90° are measured (80° in Fig.S9). This is in agreement with the angle $\alpha = 51°$ of individual chains after the first activation step (see scheme in Fig.5c).

Network orientation on the Au(100) surface

The atomic rows of the Au(100) surface represent a one-dimensional corrugation that leads not only to straight and parallel molecular chains after the first activation step, but also to a

preferential orientation of the final networks (Fig.S10). It is found that the dominant network orientation corresponds to network diagonals that are parallel to the atomic rows of the substrate (i.e. the individual chains within the network are approximately 45° off the Au(100) atomic rows) as illustrated in the inset of Fig.S10.

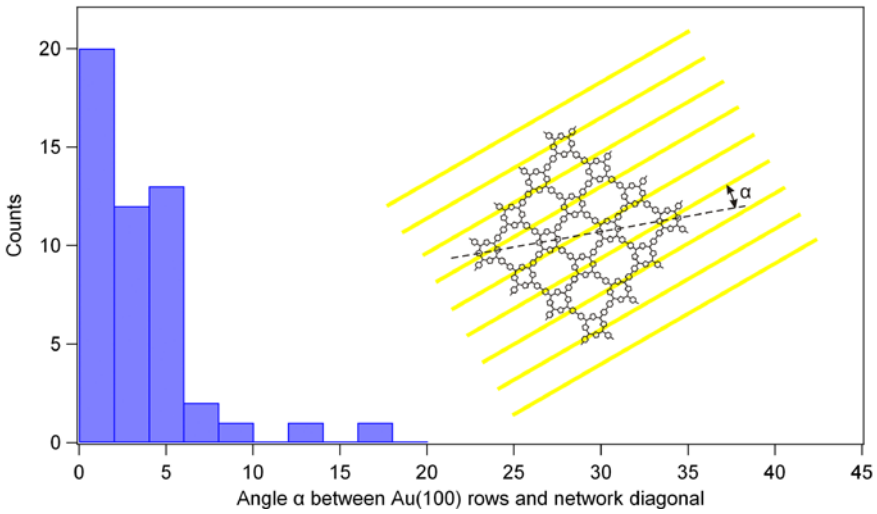

Figure S10: Histogram of the network orientation on the Au(100) surface.

References

1 Lindsey, J. S., Littler, B. J. & Wagner, R. W. *J. Org. Chem.* **64**, 1391 (1999).

2 Temelli, B. & Unaleroglu, C. *Tetrahedron.* **62**, 10130 (2006).

3 Lindsey, J. S. & Littler, B. J. *J. Org. Chem.* **64**, 2864 (1999).

4 Iancu, V., Deshpande, A. & Hla, S.-W. Manipulating Kondo temperature via single molecule switching. *Nano Letters* **6**, 820-823 (2006).

5 Grill, L. *et al.* Nano-architectures by covalent assembly of molecular building blocks. *Nature Nanotech.* **2**, 687-691 (2007).

6 Whitesides, G. M. & Grzybowski, B. Self-assembly at all scales. *Science* **295**, 2418-2421 (2002).

7 Binnig, G. K., Rohrer, H., Gerber, C. & Stoll, E. Real-space observation of the reconstruction of Au(100). *Surf. Sci.* **144**, 321-335 (1984).

8 Havu, P., Blum, V., Havu, V., Rinke, P. & Scheffler, M. Large-scale surface reconstruction energetics of Pt(100) and Au(100) by all-electron density functional theory. *Phys. Rev. B* **82**, 161418 (2010).